Technische Universität München
Fakultät für Physik

Abschlussarbeit im Bachelorstudiengang Physik

Effects of 3D Error Fields on Particle Transport in Tokamak Plasmas

Auswirkungen von 3D Störfeldern auf den Teilchentransport in Tokamakplasmen

Lukas Krumpeck

21st September 2018

Max-Planck-Institut für Plasmaphysik

Erstgutachterin: Hon.-Prof. Dr. Sibylle Günter
Zweitgutachter: Apl. Prof. Dr. Ewald Müller
Betreuer: Dr. Matthias Hölzl

Contents

Introduction

Reaching sufficient plasma confinement inside a tokamak is essential for thermonuclear fusion processes to occur at a rate necessary to use fusion as an efficient energy source. However, magnetically confined plasmas tend to develop instabilities, which impose an upper limit on the confinement. One of these instabilities, which is particularly important for the efficiency of future fusion reactors, is the edge localized mode (ELM).

ELMs periodically cause a significant loss of plasma energy and can lead to high energy fluxes to plasma facing components, potentially reducing their lifetimes considerably. It has been shown that the application of resonant magnetic perturbation fields (RMPs) by dedicated coils can mitigate or even fully suppress ELMs. However, RMP application can deteriorate plasma confinement, causing a so-called density pump-out. Although this pump-out effect has been observed in all major tokamak experiments, the observations are not consistent with predictions from simulations and the exact mechanisms driving the pump-out are not yet fully understood.

The polarization drift, a form of inertial drift which is often neglected in magnetohydrodynamic (MHD) simulations, may be a contributing factor for the observed particle transport. In cylindrical geometry, polarization drift effects have already been shown to affect density transport when RMPs are applied.

In this thesis, the effects of RMPs on particle transport are studied for toroidal plasmas using the non-linear MHD code JOREK. In particular, the influence of polarization drift effects on the plasma density profile is analyzed. The effect was studied for different perturbation amplitudes and different background particle diffusivities.

Chapter 1

Background

Generating enough usable energy to satisfy growing power demands is a pressing problem for today's society. Fossil fuels still provide about 85% of the world's total consumed energy [1].However, environmental concerns regarding this kind of energy source, such as the effects on the climate due to extensive carbon dioxide emission, are growing.

Therefore, research in alternatives to fossil fuels is becoming more important. One such alternative, which has been the topic of extensive research since the 1950's, is nuclear fusion. The energy output of a nuclear fusion reaction is significantly higher than that of nuclear fission, not to mention that of chemical processes such as the oxidation of carbon. For instance, the fusion of the hydrogen isotopes deuterium and tritium leads to a thermal energy output of approximately 3.5 MeV per nucleon, whereas the fission of uranium-235 only leads to an output of approximately 0.85 MeV per nucleon [1]. Deuterium–tritium fusion is the most promising process as an energy source in the near future due to its relatively high cross section at low energies.

Nuclear fusion can be achieved by shooting particles at a target in an accelerator, but in that case Coulomb scattering with the targets electrons would dominate and significantly reduce the efficiency as an energy source. In order for fusion processes to occur at an acceptable level, the particles have to be in thermal equilibrium, such that a lot of elastic scattering processes occur before it comes to fusion. To reach temperatures where so-called thermonuclear fusion can occur, the gas of particles has to be heated to sufficiently high energies. This leads to an ionization of the gas given by the Saha equation:

$$\frac{n_i}{n_n} \approx 3 \cdot 10^{27} \frac{T^{\frac{3}{2}}}{n_i} e^{-\frac{W_{ion}}{T}},$$

which gives an approximation for the ratio of ion (n_i) to neutral number density (n_n). Here T is the temperature and W_{ion} the ionization energy of the medium. Such a partially or fully ionized gas is then called "plasma", which is characterized

by collective effects due to the long ranging electromagnetic forces that significantly alter the properties of the gas. For instance, since the charged particles inside a plasma are able to move freely, the plasma is conductive and a relative motion of electrons and ions leads to currents inside the plasma, which themselves affect the magnetic topology of the plasma. In order for these collective effects to dominate the behavior of the gas, the degree of ionization,

$$X = \frac{n_i}{n_n + n_i},$$

has to be sufficiently high (see for example ref. [2]).

A plasma has the important property that internal charges are shielded by a local polarization of the surrounding plasma. This polarization ensures that, although on a microscopic scale the plasma consists of charged particles, on a macroscopic scale it remains neutral. This characteristic property is called quasi-neutrality and is an important principle in plasma physics (see also sec. 1.5.1). The characteristic length over which charges are shielded inside a plasma is given by the so-called Debye length,

$$\lambda_D = \sqrt{\frac{\epsilon_0 k_B T_e}{e^2 n_e}}.$$

Thus, a medium is only called plasma if the total length scale of the system is much greater than the Debye length.

In most cases the motion of single particles inside a plasma is not relevant to the overall plasma behavior. On macroscopic scales, the collective effects of the plasma outweigh any single particle motions, which leads to the approach of considering the evolution of volume elements instead of single particles analogous to hydrodynamics. However, in contrast to hydrodynamics the electric and magnetic fields lead to complicated effects due to the Lorentz force. These effects are described by the theory of magnetohydrodynamics (MHD). The most important variables describing a plasma state in MHD are the moments of the distribution function, i.e. the electron and ion densities ρ_e and ρ_i, temperatures T_e and T_i, and fluid velocities v_e and v_i, which all have to be evolved in time (see for example ref. [3, 4]).

1.1 Tokamak

In order to achieve and maintain the temperatures needed for thermonuclear fusion, the generated plasma has to be confined sufficiently well. Since a plasma consists of charged particles, it can in principle be confined using magnetic fields. After experiments with so-called pinches, which use a cylindrical configuration with magnetic mirrors at both ends to confine a plasma (see ref. [2]), toroidal

configurations were tried in the 1950s in order to achieve better plasma confinement [1].

One such device developed in the former Soviet Union is the so-called tokamak. It uses a field configuration where the magnetic field lines run helically around a torus, with the safety factor $q = \lim_{l\to\infty}(n_t/n_p)$ denoting the ratio of toroidal turns to poloidal turns of a field line (l: length over which the field line is followed). A tokamak is typically operated with a safety factor greater than one for stability purposes. The helical field is generated by superimposing a toroidal magnetic field generated by coils outside the plasma chamber and a poloidal field generated by inducing a toroidal current inside the plasma, which in turn induces a magnetic field in poloidal direction. This configuration leads to an improved plasma confinement not achievable with linear devices, where losses at the ends of the cylinder are unavoidable. Since the plasma current is usually induced by using the plasma itself as the secondary coil of a transformator, the operation of a tokamak is inherently pulsed.

Plasma inside magnetic confinement configurations, such as a tokamak, tends to be unstable due to ideal or non-ideal, e.g. resistive, MHD effects. This leads to self-amplifying perturbations of the equilibrium state, known as plasma instabilities. These instabilities impose upper boundaries on the ratio of plasma pressure to magnetic pressure,

$$\beta = \frac{p}{p_B} = \frac{p}{B^2/2\mu_0},$$

which is an important measure of magnetic confinement [1]. A high value of β, which means a high plasma pressure, is desireable as it corresponds to a low amount of magnetic energy needed to confine the plasma. In order to enhance MHD stability, additional poloidal fields are used to change the elongation and triangularity of the plasma. This also leads to the so-called X-point geometry, shown in fig. 1.1. A current in an outside conductor parallel to the plasma current causes the poloidal magnetic field to cancel to zero at the X-point, defining the separatrix which separates closed flux surfaces in the core plasma region from open flux surfaces in the outer region (see fig. 1.1). This enables a so-called divertor configuration, where the exhaust of plasma material towards the walls of the surrounding vessel is limited to a controlled target region (divertor targets).

Plasma instabilities and their consequences are an important research topic and understanding them is essential for the functionality and operating efficiency of future fusion reactors such as ITER, which is currently in construction in southern France.

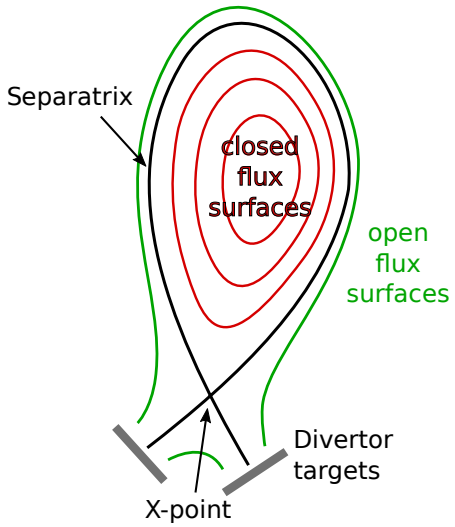

Figure 1.1: Poloidal cut through an X-point plasma. The poloidal magnetic field is zero at the X-point, leading to closed flux surfaces inside the separatrix (black line) and open flux surfaces outside the separatrix, which end at the divertor target plates.

For a consistent mathematical description of the plasma state inside a tokamak, the plasma is decomposed into its Fourier components in toroidal (mode number n) and poloidal (mode number m) direction. Since the plasma is almost axisymmetric, the n=0 mode is typically dominating. However, higher mode numbers become important for any perturbations of the axisymmetric plasma, particularly when looking at plasma instabilities such as ELMs (see sec. 1.2), which can include high mode numbers.

1.2 H-mode and ELM

The divertor configuration of a tokamak plasma lead to the discovery of the so-called high confinement mode, or H-mode [5]. When heated to a certain point, the plasma can spontaneously transition from a low confinement state (L-mode) to a high confinement state [1]. The H-mode is characterized by a significant reduction of edge plasma turbulence and a high edge pressure gradient, leading to the formation of a so-called edge pedestal. Figure 1.2 shows a comparison of the pressure profiles in H- and L-mode plasmas.

The edge pressure gradient usually grows until a so-called edge localized mode (ELM) occurs. ELMs are caused by ideal MHD instabilities which lead to periodic

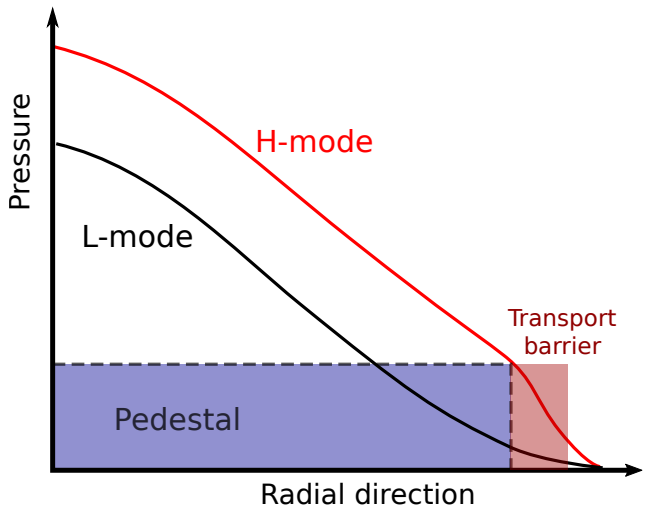

Figure 1.2: Schematic comparison of the pressure profiles in L- and H-mode plasmas. The transition from L-mode (black) to H-mode (red) leads to the formation of a transport barrier, where turbulence is suppressed. Consequently, the edge pressure gradient increases, while leaving the core profile mostly unchanged (pedestal).

releases of plasma energy. Due to the increase of the pedestal pressure gradient, the plasma crosses the ideal MHD stability limit. The plasma stability is limited due to the formation of so-called ballooning modes driven by the edge pressure gradient, peeling modes driven by edge currents (bootstrap currents) induced by the edge pressure gradient, or peeling-ballooning modes driven by both edge pressure gradient and bootstrap current [6]. The unstable MHD modes grow exponentially until the so-called "ELM crash phase" causes significant energy transport, which reduces the edge pressure gradient and thus removes the drive of the instability. This allows the edge pedestal to rebuild and the ELM cycle is repeated. The relevant plasma confinement time for ELMs is the rebuilding time of the pedestal after a previous ELM crash and is proportional to the inverse ELM frequency: $\tau_E \sim 1/f_{ELM}$. Typically these timescales are in the range of several tens of microseconds.

ELMs significantly limit the plasma confinement and cause high energy fluxes to the divertor, potentially damaging the divertor target plates. Mitigating or suppressing ELMs is particularly important for future fusion reactors such as ITER since it is estimated that ELMs will lead to an energy loss of about 10% of the total thermal energy per ELM [6]. The resulting energy flux density to the divertor target plates is believed to be significantly higher than in current experiments. Thus, in

order to avoid reduced lifetimes of these targets, the ELM amplitude has to be controlled to be below 0.7 MJ per ELM [7]. There is experimental evidence that the total ELM energy loss is mostly independent of the ELM frequency, which means increasing the ELM frequency can be used to reduce energy losses per ELM and as a result the heat loads to the divertor [6]. ELMs can be artificially triggered by inserting frozen hydrogen pellets into the plasma [8] or applying vertical kicks [9], i.e. rapidly changing the vertical position of the plasma. Another method to increase the ELM frequency or even fully suppress ELMs is to apply external magnetic perturbation fields, which will be discussed in further detail in sec. 1.4. In addition to reducing the heat load to the divertor, controlling the amplitude and frequency of ELMs can help flush out impurities of the plasma and thus improve the overall efficiency of a future fusion power reactor.

There are a number of non-linear MHD codes capable of simulating ELM crashes, such as M3D-C1, BOUT++, NIMROD or JOREK [10–16]. However, simulating the full ELM cycle starting from a stable equilibrium state has not yet been achieved in realistic simulations [6], but proof of principle has been shown in [17]. The simulations reproduce characteristic features of ELM crashes observed in experiments such as the formation of filaments, which lead to convective density exchange between the high-density pedestal region and the low-density scrape-off layer (SOL) outside the core plasma region.

1.3 Tearing Modes

Another type of MHD instabilities, called tearing modes, arises from a non-zero resistivity of the plasma. With non-zero resistivity, the plasma is not bound to the magnetic field lines. This destabilizes states which are stable in ideal MHD and leads to reconnections of field lines, a "tearing" of magnetic flux surfaces. Tearing modes can occur at flux surfaces with a rational safety factor q (see sec. 1.1). The reconnection leads to the development of magnetic islands (see fig. 1.3 and fig. 3.1), which are regions topologically disconnected from the rest of the plasma. Tearing modes are caused by the current gradient in the plasma. They can cause degradation of plasma confinement and even disruptions, which leads to a total loss of the plasma [18, 19].

1.4 Resonant Magnetic Perturbations

As mentioned in sec. 1.2, the ELM frequency can be increased by applying external magnetic perturbation fields, which decreases the energy loss per ELM. These perturbation fields are generated by in-vessel or ex-vessel coils, which are distributed

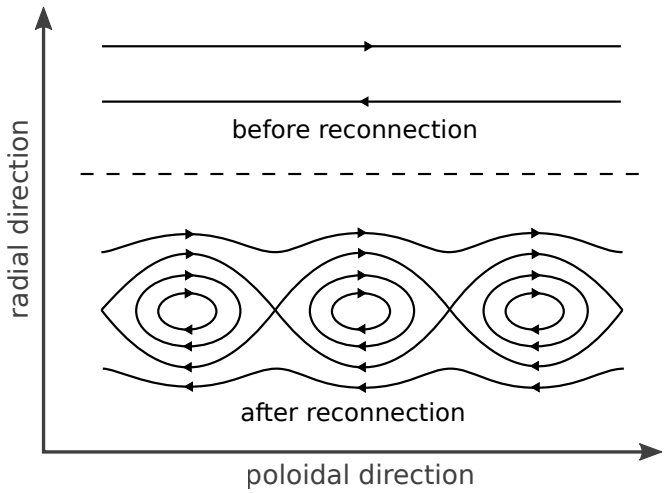

Figure 1.3: Schematic depiction of the reconnection caused by tearing modes. Without perturbation, the flux surfaces are parallel to each other. An internal or external perturbation can lead to reconnection of field lines and thus to the formation of a magnetic island with nested flux surfaces (cf. X-point configuration in fig. 1.1). The arrows point in the direction of the poloidal magnetic field.

in typically two or three poloidal rows around the torus [20]. The number of toroidal coils determines the highest mode number n that can be applied, whereas the number of poloidal coils helps control the phase of the perturbation and the spectrum of accessible poloidal m-modes. If a flux surface with safety factor $q = m/n$ lies within the plasma, the magnetic perturbation is called resonant magnetic perturbation (RMP) [21]. RMPs cause a global plasma response, for example deformation of flux surfaces, magnetic island formation or a deceleration of the plasma rotation, depending on parameters such as the RMP amplitude and phase and the plasma rotation and resistivity [18, 19, 22].

Experiments at various tokamak reactors, such as DIII-D, JET, MAST, KSTAR, EAST and ASDEX Upgrade, have shown that RMPs are a robust way to mitigate or suppress ELMs [20]. At DIII-D complete ELM suppression was achieved in ITER relevant regimes, with small $n = 3$ RMPs [23]. In ASDEX Upgrade the suppression was reproduced for DIII-D-similar plasmas with high triangularity [24]. In other regimes ELMs were mitigated using $n = 2$ perturbations [25]. At JET and MAST, which both use a similar arrangement of perturbation coils, complete ELM suppression was not achieved [26]. However, the ELM amplitude and energy was reduced and the frequency increased in both experiments. On MAST, for instance,

ELMs were mitigated by applying $n = 3, 4$ or 6 perturbations. The ELM frequency increased by a factor of 8 with similar reduction of the energy loss [27].

Together with injection of frozen deuterium-tritium pellets, applying RMPs will be the main method of controlling ELMs at ITER. A set of 27 coils is planned to be installed in three rows inside the vacuum vessel [6]. In order to keep the energy loss per ELM at an acceptable level, the frequency of ELMs has to be at least increased by a factor of 30 using the RMP coils, but full ELM suppression will probably be mandatory. The extrapolation of current RMP experiments to ITER conditions turns out to be difficult since the expected plasma properties at ITER, with low collisionality and high relative density at the same time, cannot be obtained in present experiments [6, 28].

1.4.1 RMP Influence on Tearing Modes

As discussed in sec. 1.3, tearing modes are normally caused by internal perturbations in the plasma, which causes magnetic field lines to reconnect. However, they can also be triggered and influenced by external magnetic perturbation fields. Perturbation fields in resonance with m/n modes, i.e. fields with the dominant n fixed by the perturbation coils, can cause magnetic reconnection and therefore the formation of magnetic islands at $q = m/n$ rational surfaces [29]. Experiments as well as simulations on ASDEX Upgrade have shown the seeding of magnetic islands by magnetic perturbations [18]. During RMP ramp-up, at first the RMP penetration is shielded until a certain threshold amplitude is reached. The perturbation causes a decrease in plasma rotation and a change in the electron perpendicular velocity ($\boldsymbol{v}_{\perp,e}$), which leads to fast reconnection of field lines and formation of magnetic islands when $\boldsymbol{v}_{\perp,e} = 0$ is reached and the island size saturates. Large magnetic islands can lead to a sudden loss of the whole plasma confinement (major disruption). Both simulation and experiment come to the conclusion that the drop of $\boldsymbol{v}_{\perp,e}$ to zero corresponds to the penetration of the perturbation fields [30].

1.4.2 Density Pump-out

The application of RMP fields is often accompanied by a reduction of the overall plasma density, which has been shown by various experiments [20, 25, 27, 31, 32]. In MAST, for instance, RMPs lead to a major density reduction of up to 35% of the total density in certain cases [32]. As described above, RMPs can cause the formation of magnetic islands. In the edge plasma region, these islands can overlap due to the high density of rational surfaces. This leads to a stochastization of field lines in the overlapping regions, which increases energy and particle transport [29, 33]. However, simulations suggest that the stochastization alone should predominantly

increase energy and not particle transport, which does not match experimental findings [6]. The increased energy transport at magnetic islands should lead to a flattening of the temperature gradient over the extent of the island. The mechanisms causing the density pump-out effect are part of ongoing research and are still not fully understood. The polarization drift, which is often neglected in non-linear MHD simulations, has been shown in cylindrical geometry to be a significant factor contributing to this effect [34, 35].

1.5 Particle Drifts

After having discussed the importance of resonant magnetic perturbations for fusion research, the following section will focus on particle drift effects to investigate whether they could be responsible for the observed density pump-out.

Charged particles in a homogeneous magnetic field are generally moving on spiral paths around magnetic field lines due to the Lorentz force,

$$\boldsymbol{F}_L = m\frac{\mathrm{d}\,\boldsymbol{v}}{\mathrm{d}t} = q(\boldsymbol{v}\times\boldsymbol{B}), \tag{1.1}$$

when no other forces are acting on them. Here q is the charge of the particle, m the particle's mass, $\boldsymbol{v}$ the velocity and $\boldsymbol{B}$ the magnetic field. This spiral motion is the superposition of a circular motion perpendicular to the magnetic field lines and motion with constant velocity parallel to the magnetic field lines, $\boldsymbol{v} = \boldsymbol{v}_\parallel + \boldsymbol{v}_\perp$. For B in z-direction, for instance, this gives:

$$\begin{aligned} v_x &= v_\perp \sin\frac{qB}{m}t \\ v_y &= v_\perp \cos\frac{qB}{m}t \\ v_z &= const. = v_\parallel. \end{aligned}$$

If there is an additional constant electric field, the equations in parallel and perpendicular directions write:

$$\begin{aligned} \frac{\mathrm{d}\,\boldsymbol{v}_\parallel}{\mathrm{d}t} &= \frac{q}{m}\boldsymbol{E}_\parallel \\ \frac{\mathrm{d}\,\boldsymbol{v}_\perp}{\mathrm{d}t} &= \frac{q}{m}\boldsymbol{v}_\perp\times\boldsymbol{B} + \frac{q}{m}\boldsymbol{E}_\perp. \end{aligned}$$

The velocity $\boldsymbol{v}_\perp$ can be split up in:

$$\boldsymbol{v}_\perp = \boldsymbol{v}_D + \boldsymbol{u},$$

such that

$$\frac{\mathrm{d}\,\boldsymbol{u}}{\mathrm{d}t} = \frac{q}{m}\boldsymbol{u} \times \boldsymbol{B},$$

which means $\boldsymbol{u}$ describes the circular motion due to the Lorentz force perpendicular to the magnetic field (cf. eq. (1.1)). This leads to a constant drift velocity:

$$\boldsymbol{v}_D = \frac{\boldsymbol{E} \times \boldsymbol{B}}{B^2},$$

commonly known as $E \times B$–drift. This mechanism can be applied to an arbitrary force $\boldsymbol{F}$ acting on the particle, leading to the general equation:

$$\boldsymbol{v}_D = \frac{\boldsymbol{F} \times \boldsymbol{B}}{qB^2}.$$

For further information on particle drifts in plasmas see for example [4]. Some notable drifts occurring in tokamak plasmas are:

- the $E \times B$ drift described above,
- the diamagnetic drift:

  $$\boldsymbol{v}^* = -\frac{\nabla P \times \boldsymbol{B}}{nqB^2},$$

  which does not occur for single particles but comes from the net particle motion in a fluid element.
- the drift caused by the curvature and gradient of the magnetic field:

  $$\boldsymbol{v}_R + \boldsymbol{v}_{\nabla B} = \frac{m}{q}\frac{\boldsymbol{R_c} \times \boldsymbol{B}}{R_c^2 B^2}\left(\boldsymbol{v}_\parallel^2 + \frac{1}{2}\boldsymbol{v}_\perp^2\right),$$

  where R_c is the curvature radius.
- inertial drifts caused by time varying forces. Time varying forces lead to a changing drift velocity, and this acceleration causes itself a new drift. The general form of inertial drifts is given by:

  $$\boldsymbol{v}_I = \frac{-m}{qB^2}\frac{\mathrm{d}\,\boldsymbol{v}}{\mathrm{d}t} \times \boldsymbol{B}.$$

  A particularly important inertial drift, caused by a time varying electric field, is the so-called polarization drift:

  $$\boldsymbol{v}_{pol} = \frac{m}{qB^2}\frac{\mathrm{d}\,\boldsymbol{E}}{\mathrm{d}t}.$$

  Since the polarization drift is proportional to the mass of the particle, it is commonly neglected for electrons. However, the ion polarization drift can be important for MHD calculations, which is shown in the next section.

1.5.1 Polarization Drift

In the following particle drifts are derived using a fluid description of the plasma and the changes made in JOREK in order to include polarization drift effects are illustrated. This section follows ref. [36]. To ensure the quasi-neutrality of a plasma at macroscopic scales, the density equation for electrons should be equal to the ion density equation. However, JOREK and many other MHD codes normally neglect inertial drifts in the ion density equation since they are small compared to other terms such as the $E \times B$–term.

The density equation for electrons and ions is given by:

$$\frac{\partial n_k}{\partial t} + \nabla \cdot (n_k \boldsymbol{v}_k) = D_\perp \nabla_\perp^2 n_k + S_{n_k},$$

where the index $k = e, i$ stands for electrons and ions, respectively. If we neglect some terms of the velocity, as it is commonly done in MHD codes, these two equations become different. The velocities for ions and electrons are derived using the momentum equations. For ions the momentum equation is given by:

$$m_i n \frac{\mathrm{d}\,\boldsymbol{v}_i}{\mathrm{d}t} = en(\boldsymbol{E} + \boldsymbol{v} \times \boldsymbol{B}) - \nabla P_i - \nabla \cdot \bar{\Pi}_i - en\eta \boldsymbol{J}. \tag{1.2}$$

Here $\boldsymbol{J} = ne(\boldsymbol{v}_i - \boldsymbol{v}_e)$ is the electrical current, $\eta = \frac{m_e \nu_{ei}}{ne^2}$ the resistivity, ν_{ei} the electron ion collision frequency, $\bar{\Pi}_i$ the pressure tensor and $n = n_i = n_e$ (quasi-neutrality). Taking the cross product of equation (1.2) with $\boldsymbol{B}$ one gets for the total ion velocity:

$$\begin{aligned}\boldsymbol{v}_i &= \boldsymbol{v}_{i,\parallel} + \boldsymbol{v}_{E\times B} + \boldsymbol{v}_i^* + \boldsymbol{v}_{i,pol} + \boldsymbol{v}_{\Pi_i} + \boldsymbol{v}_\eta \\ &= \boldsymbol{v}_{i,\parallel} + \frac{\boldsymbol{E}\times\boldsymbol{B}}{B^2} - \frac{\nabla P_i \times \boldsymbol{B}}{neB^2} - \frac{m_i}{eB^2}\frac{\mathrm{d}\,\boldsymbol{v}_{E\times B}}{\mathrm{d}t} \times \boldsymbol{B} - \frac{\nabla \cdot \bar{\Pi}_{i,\mathrm{neo}} \times \boldsymbol{B}}{neB^2} - \frac{\eta \boldsymbol{J} \times \boldsymbol{B}}{B^2}.\end{aligned}$$

Here $\boldsymbol{v}_i^*$ represents the diamagnetic drift, $\boldsymbol{v}_{i,pol}$ the polarization drift, $\boldsymbol{v}_{\Pi_i}$ neoclassical effects and $\boldsymbol{v}_\eta$ the drift caused by a non-zero resistivity of the plasma. The ion inertial drift velocity was approximated to its first order ($\boldsymbol{v}_{i,pol}$) and the gyroviscous cancellation [36],

$$\frac{\mathrm{d}\,\boldsymbol{v}_i}{\mathrm{d}t} \times \boldsymbol{B} \approx -\nabla \cdot \bar{\Pi}_{i,gv} \times \boldsymbol{B},$$

was used. For the MHD ordering, all terms except $\boldsymbol{v}_{i,\parallel}$ and $\boldsymbol{v}_{E\times B}$ are neglected. The two-fluid ordering [37] used in JOREK (see sec. 1.6) includes also $\boldsymbol{v}_i^*$ since in this case it is of the order of $\boldsymbol{v}_{E\times B}$. The extension of JOREK added by François Orain [36] additionally keeps ion inertial drifts up to first order to ensure the consistency of the density equations.

The electron velocity is derived similarly, but in addition to the approximations made for the ion velocity, the neoclassical term is also neglected. Thus the electron velocity is given by:

$$\boldsymbol{v}_e = \boldsymbol{v}_{e,\parallel} + \frac{\boldsymbol{E}\times\boldsymbol{B}}{B^2} + \frac{\nabla P_e \times \boldsymbol{B}}{neB^2}.$$

Plugging this in the density equation and using $\boldsymbol{v}_{e,\parallel} = -\frac{\boldsymbol{J}_\parallel}{ne} + \boldsymbol{v}_{i,\parallel}$ leads to the complete density equation for electrons:

$$\frac{\partial n}{\partial t} + \boldsymbol{v}_{E\times B}\cdot\nabla n - \frac{1}{e}\nabla\cdot\boldsymbol{J}_\parallel + \nabla\cdot\left(n\boldsymbol{v}_{\parallel,i}\right) + n\left(\nabla u - \frac{\nabla P_e}{ne}\right)\cdot\left(\nabla\times\frac{\boldsymbol{B}}{B^2}\right) = \\ = D_\perp\nabla_\perp^2 n + S_n.$$

Since electron and ion density equations can be shown to be equivalent (full derivation in [36]) only one of them has to be implemented. Thus, the only changes made to the ion density equation already implemented in JOREK,

$$\frac{\partial n}{\partial t} + \boldsymbol{v}_{E\times B}\cdot\nabla n + \nabla\cdot\left(n\boldsymbol{v}_{\parallel,i}\right) + n\left(\nabla u + \frac{\nabla P_i}{ne}\right)\cdot\left(\nabla\times\frac{\boldsymbol{B}}{B^2}\right) = D_\perp\nabla_\perp^2 n + S_n,$$

were to add a term $-\frac{1}{e}\nabla\cdot\boldsymbol{J}_\parallel$ and to replace the ion pressure P_i by $-P_e$. Furthermore, the term $P\nabla\cdot\boldsymbol{v}$ in the energy and momentum equations was changed to include a polarization term $P\nabla\cdot\boldsymbol{v}_{pol}$ and a neoclassical term $P\nabla\cdot\boldsymbol{v}_{\Pi_i}$.

In cylindrical geometry, it has already been shown that the polarization drift causes density pump-in or pump-out, depending on the configuration [34]. However, it has not yet been confirmed with toroidal codes such as JOREK.

1.6 JOREK

The effects of the polarization drift term on particle transport were studied by running computer simulations with the non-linear MHD-code JOREK. JOREK has already been used to study various aspects of tokamak plasmas [6, 15, 16, 29, 37]. The main applications of JOREK are core and edge instabilities such as tearing modes and ELMs. It is capable of simulating plasmas with realistic X-point geometry using flux aligned grids for the calculations. JOREK includes mostly reduced MHD models (sec. 1.6.1), but also a full MHD model is in development. For the simulations for this thesis we used a side-branch of JOREK not yet integrated in the main code, which was extended to include the polarization drift as described in sec. 1.5.1.

1.6.1 Reduced MHD model

The polarization drift extension was added to "model 303" of the JOREK code. Model 303 is a reduced MHD model, assuming that the toroidal field is constant in time, and includes neoclassical effects, diamagnetic effects and toroidal flows. For further information about the reduced MHD model used for JOREK see [37]. The model was extended in 2014 to ensure a consistent density equation, as described above, but not yet thoroughly tested, which was the main goal of this thesis. A test case was set up with the TM1.f code to be able to compare effects caused by the polarization drift during RMP application.

1.6.2 TM1.f

The code TM1.f, developed by Dr. Qingquan Yu, was originally based on the two-fluid equations in cylindrical geometry with periodic boundary conditions. In this cylindrical geometry, TM1.f has found an influence of the polarization drift on the density profile when RMPs were applied [34]. Recently the code has been expanded to include toroidal mode coupling. The goal of this thesis was to set up a case which can be calculated by both TM1.f and JOREK and then study this test case extensively such that it can be compared later on. The exact comparison has to be left for future studies since the TM1.f code has only recently been extended to toroidal geometry and is also not yet tested sufficiently for this geometry yet.

As opposed to JOREK, TM1.f can only simulate plasmas with shifted circular magnetic surfaces and uses the large aspect ratio approximation for the toroidal geometry. TM1.f includes advanced two-fluid physics and has been used to study RMP physics, forced reconnection, sawtooth crashes, the non-linear growth of neoclassical tearing modes and their stabilization by electron cyclotron current drive [34, 38–41].

Chapter 2

Setting up Simulation

The goal of this thesis was to set up a test case which can be simulated by both JOREK and TM1.f for benchmarking ion polarization drift effects during RMP application, and to study effects on the density profile. The test case was kept simple to keep the necessary computation time low, such that a number of different simulations could be run.

2.1 Geometry

The benchmark case consists of a plasma with toroidal geometry and circular cross section. The aspect ratio was chosen to be 5, with a minor radius of $a = 0.5\,\mathrm{m}$ and a major radius of $R_0 = 2.5\,\mathrm{m}$. Due to the toroidal geometry, the projection of the equilibrium magnetic flux surfaces on the poloidal plane are circles shifted towards the low field side.

JOREK uses cylindrical coordinates to parametrize the plasma, whereas TM1.f uses straight field line coordinates. The position of the RMP coils in JOREK is defined using the poloidal angle θ, in the TM1.f code via the poloidal-like straight field line angle θ^*. In first order these angles are related by:

$$\theta = \theta^* - \left(\frac{\mathrm{d}\,\Delta}{\mathrm{d}r} + \frac{r}{R}\right)\sin\theta^*,$$

where Δ is the shift of the magnetic axis.

2.2 Plasma Parameters

A deuterium plasma was chosen for this benchmark case, with the ion mass $m_i = 2m_p$, where m_p is the mass of the proton. The central particle density n_0 was set to $10^{19}\,\mathrm{m}^{-3}$. A toroidal magnetic field with a magnitude of $2\,\mathrm{T}$ was used. The electron and ion temperatures T_e and T_i were set to be constant in both space and time, with $T_e = T_i = 400\,\mathrm{eV}$. To ensure this the energy equation implemented in JOREK was switched off. The ratio of specific heats, γ, was set to 1. The resistivity,

η, and viscosity, μ, of the plasma where chosen to be constant in space and time, with $\eta = 1.1 \times 10^{-5}\,\Omega\,\mathrm{m}$ and $\mu = 0.2 \times 10^{2}\,\mathrm{m}^2/\mathrm{s}$. The perpendicular particle diffusivity, $D_\perp$, was also set to be spatially and temporally constant, with different values of $0.04\,\mathrm{m}^2\mathrm{s}^{-1}$, $0.12\,\mathrm{m}^2\mathrm{s}^{-1}$ and $0.4\,\mathrm{m}^2\mathrm{s}^{-1}$ chosen to study the influence of the diffusivity on the particle transport.

Diamagnetic terms in JOREK are controlled via the input parameter τ_{IC} defined by:

$$\tau_{IC} = \frac{m_i}{2eF_0\sqrt{\mu_0\rho_0}},$$

where $F_0 = B_{axis} \cdot R_{axis}$ and ρ_0 is the central mass density. A value for τ_{IC} of 1.01×10^{-2} was used.

2.3 Input Profiles

In JOREK, all input profiles are given in terms of the normalized magnetic flux $\Psi_N = \Psi/(\Psi_{axis} - \Psi_{boundary})$, whereas TM1.f uses the minor radius r for the parametrization. The relationship between r and Ψ_N is shown in fig. 2.1.

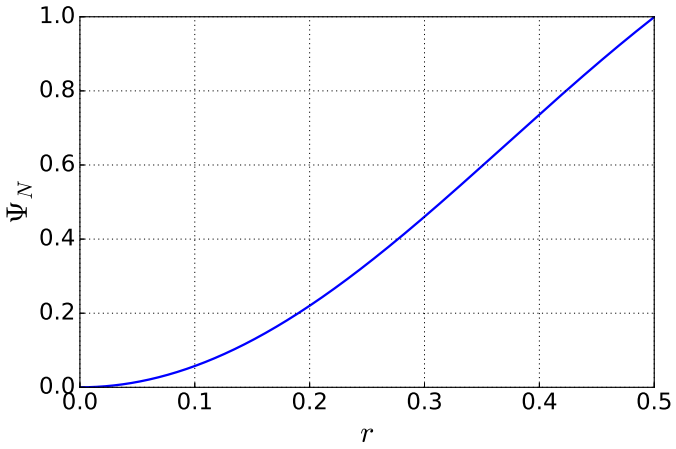

Figure 2.1: Normalized magnetic flux Ψ_N as a function of the minor radius r.

The equilibrium plasma density used for the calculations, normalized to the central density, is given by:

$$\frac{n_e}{n_{e,0}} = 0.8\left[1 - \left(\frac{r}{a}\right)^2\right]^2 + 0.2,$$

which is illustrated in fig. 2.2. A poloidal background rotation profile as shown in fig. 2.3 was used.

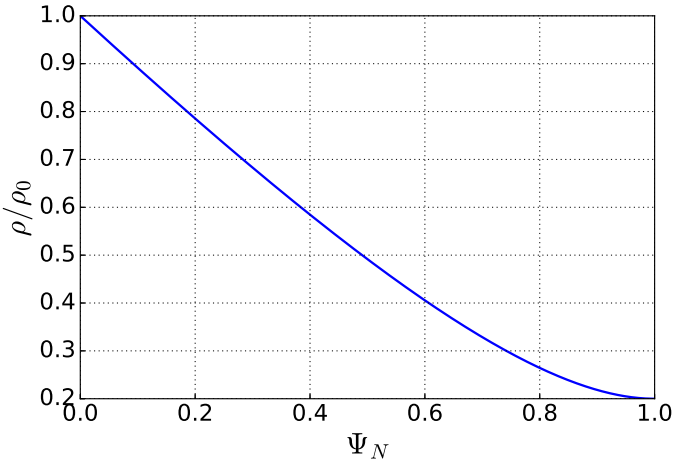

Figure 2.2: Equilibrium plasma density profile as a function of the normalized magnetic flux.

Another input parameter which had to be adapted in JOREK was the $FF' = F\,\mathrm{d}F/\mathrm{d}\Psi$ profile, which is needed to solve the Grad-Shafranov equation:

$$\Delta^*\Psi = -\mu_0 R^2 \frac{\mathrm{d}\,p}{\mathrm{d}\Psi} - F\frac{\mathrm{d}\,F}{\mathrm{d}\Psi},$$

where Ψ is the poloidal magnetic flux, μ_0 is the vacuum permeability and $F = RB_\Phi$ is the poloidal current stream function (B_Φ is the magnetic field in toroidal direction). The profile was calculated using the input parameters and the q-profile used for the TM1.f simulation and then slightly adjusted to align the q-profiles of JOREK and TM1.f. Figure 2.4 shows the equilibrium q-profile for JOREK, with $q_0 = 1.0$ and $q_a = 2.4$.

2.4 RMP Application

For the case studied, a resonant magnetic perturbation with $m/n = 3/2$ was applied in the straight field line coordinate system of TM1.f. The amplitude was varied from approximately $1.784 \times 10^{-9}\,\mathrm{Tm}^2$ to $3.0 \times 10^{-4}\,\mathrm{Tm}^2$ to study RMP penetration and their impact onto the density profile.

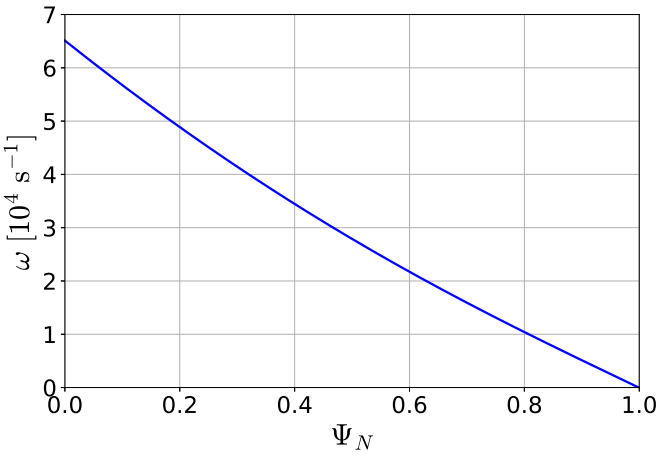

Figure 2.3: Poloidal plasma rotation ω as a function of the normalized magnetic flux Ψ_N.

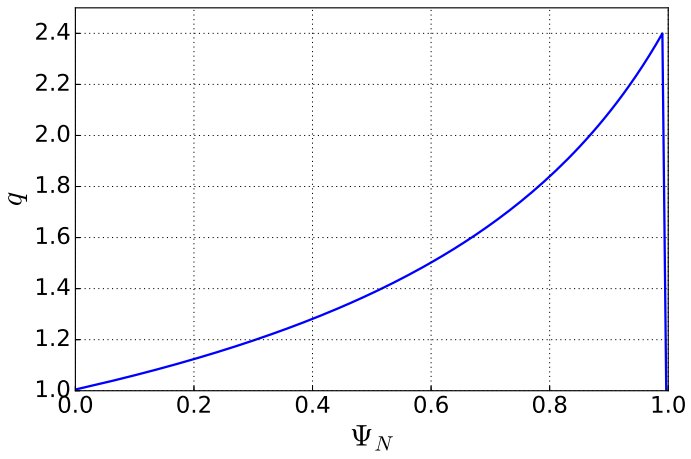

Figure 2.4: Profile of the safety factor q for the test case.

Chapter 3

Results

In order to study the effects of the polarization drift on particle transport during RMP application, a number of different simulations were performed. Table 3.1 lists all of these simulations. All simulations in JOREK were carried out with and without polarization drift effects considered (corresponding to columns A and B in tab. 3.1), and also with and without considering diamagnetic effects (C). This was done by setting the parameter τ_{IC} to 0 for some simulations. Since setting τ_{IC} to zero also switches off the polarization current, three different configurations were analyzed. The perpendicular particle diffusivity (sec. 2.2) was also varied between $0.04\,\mathrm{m^2s^{-1}}$ and $0.4\,\mathrm{m^2s^{-1}}$ in order to study its effects on the density profile in steady state after RMP application.

$D_\perp$ [$\mathrm{m^2s^{-1}}$] / Ψ_{RMP} [$\mathrm{Tm^2}$]	0.04			0.12			0.4		
	A	B	C	A	B	C	A	B	C
1.8×10^{-8}								X	
3.6×10^{-8}							X	X	
1.8×10^{-7}							X	X	X
3.6×10^{-7}							X	X	
8.9×10^{-7}								X	
1.8×10^{-6}	X	X	X	X	X	X	X	X	X
5.4×10^{-6}	X	X	X	X	X	X	X	X	X
1.1×10^{-5}	X	X	X	X	X	X	X	X	X
1.8×10^{-5}	X	X	X	X	X	X	X	X	X
2.4×10^{-5}								X	
3.6×10^{-5}							X	X	X
7.1×10^{-5}	X	X					X	X	
1.8×10^{-4}							X	X	X
3.6×10^{-4}							X	X	X

Table 3.1: List of all non-axisymmetric simulations done for this thesis. The first row lists the different perpendicular diffusivities $D_\perp$, the first column lists the different RMP amplitudes Ψ_{RMP}. The letters A–C represent the three analyzed configurations, namely: A—with diamagnetic and polarization drifts; B—with diamagnetic effects, but without polarization drift; C—without diamagnetic and polarization drift effects($\tau_{IC} = 0$). The crosses show which simulations were performed for the respective configurations.

3.1 Simulations

All cases were simulated long enough to reach steady state. Axisymmetric simulations were carried out as well for comparison. For the non-axisymmetric simulations, only the toroidal mode numbers 0 and 2 where calculated. To verify that the plasma state is stable in JOREK without RMP application a non-axisymmetric simulation with RMPs disabled was performed, which showed that the $n = 2$ mode is stable without RMP. For all other simulations where RMPs were enabled, the RMP amplitude was ramped up over a timescale of one millisecond according to a hyperbolic tangent function. The steady state solution was achieved after a timescale of 10^2 to 10^3 ms (see fig. 3.3).

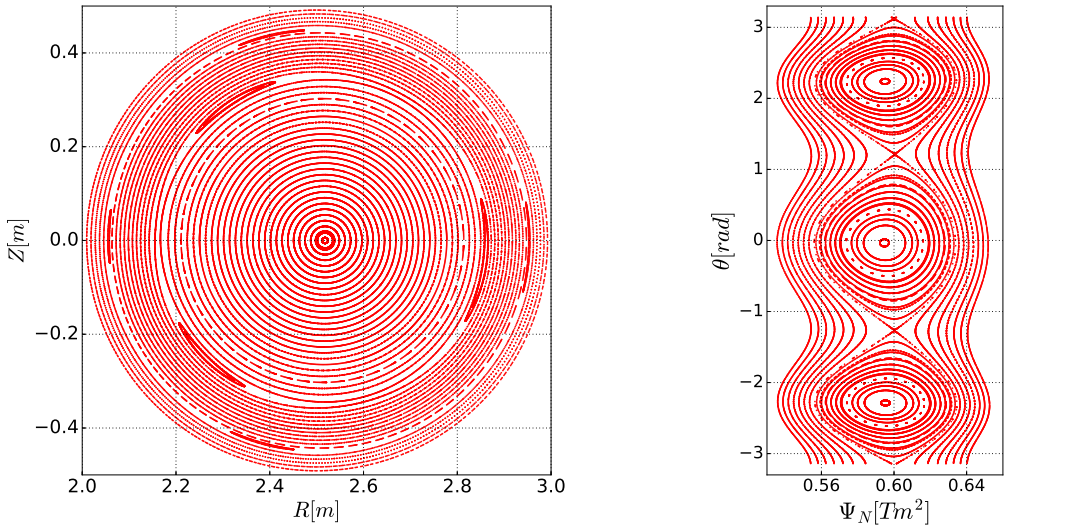

(a) Poloidal cut through the plasma with clearly visible magnetic islands at the 3/2 and 4/2 rational surfaces.

(b) Close-up of the 3/2 magnetic island where the magnetic flux Ψ_N is plotted against the poloidal angle θ.

Figure 3.1: Poincare plots of the plasma profile with an RMP amplitude of $\Psi_{RMP} = 1.8{\cdot}10^{-4}$.

3.2 Penetration of RMPs

To examine the effects of the amplitude of the applied RMPs on the plasma (see sec. 1.4), a scan over the RMP amplitude was performed.

As discussed in sec. 1.4, the applied RMP field leads to the formation of magnetic islands at the 3/2 and also at the 4/2 rational surfaces, due to the construction of the q-profile with $1 < q < 5/2$. Figure 3.1 shows Poincaré plots of the plasma cross section for one particular simulation, with $\Psi_{RMP} = 1.8 \times 10^{-4}\,\mathrm{Tm}^2$, $D_\perp = 0.4\,\mathrm{m}^2\mathrm{s}^{-1}$, and without considering polarization drift effects (B). The magnetic field lines are followed for a fixed number of turns around the torus and every intersection with the chosen poloidal plane is represented by a point in the plot. Therefore the lines seen in fig. 3.1 represent closed magnetic flux surfaces. In the region of the 3/2 island, for instance, these surfaces have reconnected due to a tearing mode and now form an island with locally nested flux surfaces.

For one particular series of simulations, column 0.4B in table 3.1, the behavior of the width of the 3/2 magnetic island was monitored with respect to the RMP amplitude. The dependence of the width on the RMP amplitude can be seen in fig. 3.2. The dashed line represents the expected behavior for a fully penetrated RMP field. The deviations from that line for small amplitudes indicates a shielding of the perturbation fields by plasma flows (see sec. 1.4.1). For large amplitudes, however, the RMP fields seem to penetrate fully and follow the dashed line, which corresponds to a square root dependence.

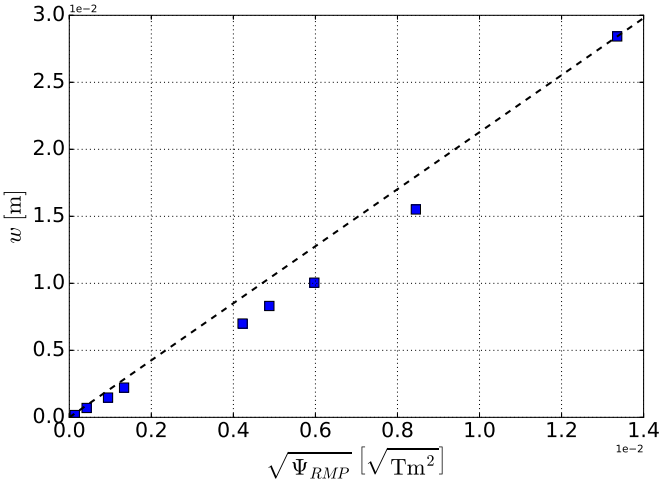

Figure 3.2: Plot of the magnetic island width w with respect to the square root of the perturbation flux. $D_\perp$ was set to $0.4\,\mathrm{m}^2\mathrm{s}^{-1}$ and only diamagnetic effects were taken into account (column "B" in tab. 3.1). The dashed line represents the expected behavior for a fully penetrated RMP field.

This corresponds also to the observed electron perpendicular velocity $v_{\perp,e}$. When an island fully penetrates, $v_{\perp,e}$ should approach zero (see sec. 1.4 and [18, 19]). In fig. 3.3 both the electron perpendicular velocity ($v_{\perp,e}$) at the 3/2 rational surface and the width of the 3/2 magnetic island (w) are shown as a function of the simulation time for two different RMP amplitudes, $\Psi_{RMP} = 1.8 \times 10^{-5}\,\mathrm{Tm}^2$ (red) and $\Psi_{RMP} = 1.8 \times 10^{-4}\,\mathrm{Tm}^2$ (blue). The particle diffusivity in this case was set to $0.4\,\mathrm{m}^2\mathrm{s}^{-1}$ and only diamagnetic effects were considered.

For high amplitudes (blue) the velocity drops to approximately zero, indicating almost full RMP penetration. For lower amplitudes (red), corresponding to the points below the dashed line in fig. 3.2, $v_{\perp,e}$ approaches non-zero values, indicating only partial penetration.

The island width (lower subplot) grows corresponding to the penetration of the RMP field, shown by $v_{\perp,e}$. Both of these results indicate that for an amplitude of $1.8 \times 10^{-4}\,\mathrm{Tm}^2$ the field has almost fully penetrated, while for lower amplitudes the rotation of the plasma partially shields the applied perturbation fields (see sec. 1.4.1).

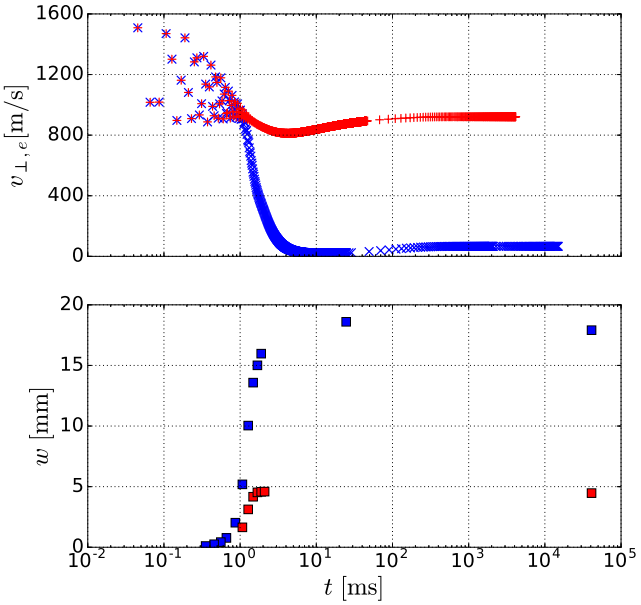

Figure 3.3: Time evolution of the electron perpendicular velocity $v_{\perp,e}$ and magnetic island width w at $q = 3/2$ for two different RMP amplitudes: red– $\Psi_{RMP} = 1.8 \times 10^{-5}\,\mathrm{Tm}^2$; blue– $\Psi_{RMP} = 1.8 \times 10^{-4}\,\mathrm{Tm}^2$. For the particle diffusivity a value of $D_\perp = 0.4\,\mathrm{m}^2\mathrm{s}^{-1}$ was used and only diamagnetic effects were considered in this case.

3.3 Effects of RMPs on Density Profile

To study the effects of RMPs on particle transport, the density profile of the steady state solution was analyzed for different island sizes and different diffusivities. For the three different configurations used (A, B and C), the axisymmetric simulations lead to almost identical steady state solutions, with slight deviations at the plasma center. To compare the different simulations, all further graphs show the respective values in relation to the corresponding axisymmetric values.

Figure 3.4 shows the gradient of the density profile, normalized to the axisymmetric density gradient, for all three different configurations. The perturbation amplitude and perpendicular diffusivity were held fixed at $\Psi_{RMP} = 1.1 \times 10^{-5}\,\mathrm{Tm}^2$ and $D_\perp = 0.04\,\mathrm{m}^2\mathrm{s}^{-1}$, leading to a width of the 3/2 magnetic islands of $w = 4.6\,\mathrm{mm}$ (A), 3.8 mm (B) and 3.4 mm (C). The influence of the RMPs can be clearly seen at the 3/2 and 4/2 rational surfaces, although the effects are much stronger at the 3/2 surface. This is consistent with the Poincaré plots in fig. 3.1, where the 4/2 magnetic island is considerably smaller than the 3/2 island. The respective island size is also shown by the shaded areas in fig. 3.4. Moreover, fig. 3.4 shows that there are significant differences of the density gradient at rational surfaces for the three different configurations. The by far strongest effects are observed when including the polarization current in the density equation (see sec. 1.5.1). Diamagnetic effects also seem to play a role, but for the chosen parameters polarization effects dominate over other influences.

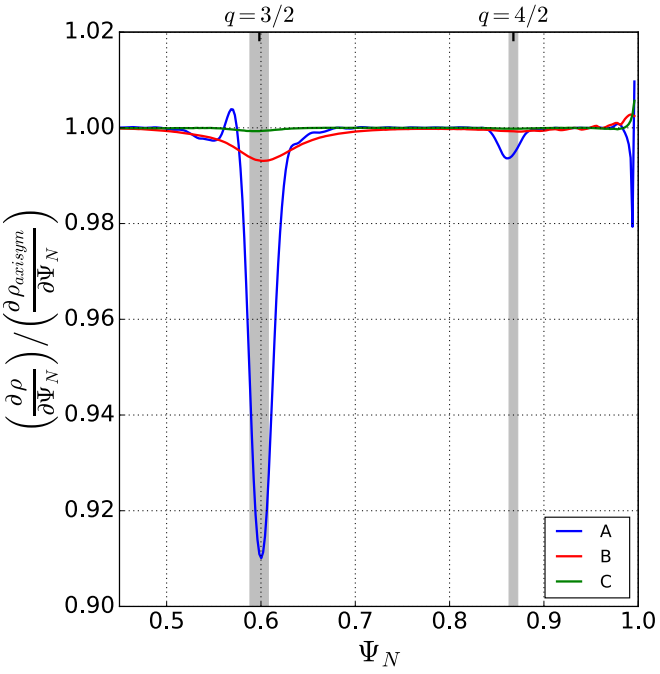

Figure 3.4: Gradient of the density profile, normalized to the density gradient of the axisymmetric simulation, as a function of the normalized magnetic flux Ψ_N for $\Psi_{RMP} = 1.1 \times 10^{-5}\,\mathrm{Tm}^2$ and $D_\perp = 0.04\,\mathrm{m}^2\mathrm{s}^{-1}$. The safety factor q marks the positions of the 3/2 and 4/2 rational surface, the shaded areas represent the extent of the respective island. The labels A, B and C represent the same configurations as in tab. 3.1.

In the following, the increase of the particle transport coefficient at the 3/2 rational surface,

$$d_{rat}^{+} = \left[1 - \left(\frac{\partial \rho}{\partial \Psi_N}\right) / \left(\frac{\partial \rho_{axisym}}{\partial \Psi_N}\right)\right]_{q=3/2} \cdot D_\perp,$$

is analyzed with respect to the diffusivity, perturbation amplitude and island width. In fig. 3.5 d_{rat}^{+} is shown for different values of the perpendicular particle diffusivity. The perturbation amplitude was kept at $\Psi_{RMP} = 1.1 \times 10^{-5}\,\mathrm{Tm}^2$. The three points at $D_\perp = 0.04\,\mathrm{m}^2\mathrm{s}^{-1}$ correspond to the three graphs shown in fig. 3.4.

When only considering background particle transport (C), the transport coefficient shows a dependence on the perpendicular particle diffusivity of the form: $d_{rat}^{+} \propto D_\perp$. Also taking diamagnetic and $E \times B$ effects (B) into account, the curve stays approximately constant, indicating that in this model d_{rat}^{+} is independent of $D_\perp$. In

the third case, considering also polarization drift effects, the transport coefficient decreases with increasing $D_\perp$, approximately of the form: $d^+_{rat} \propto 1/D_\perp$.

This also means that the relative importance of polarization and diamagnetic effects with respect to the background particle transport decreases as $1/D^2_\perp$ and $1/D_\perp$, respectively.

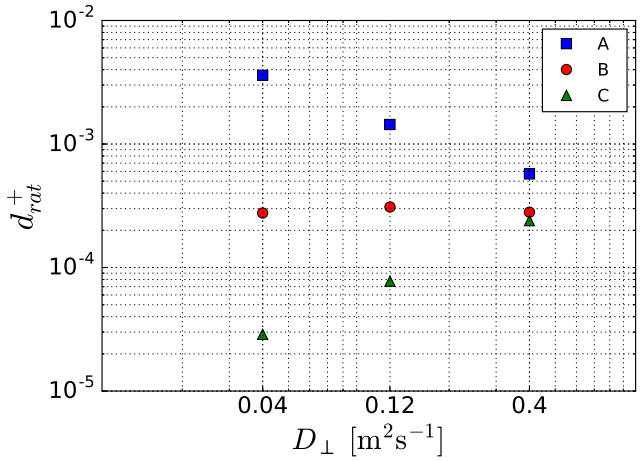

Figure 3.5: The normalized density gradient as a function of the perpendicular particle diffusivity $D_\perp$, with logarithmic scales on both axes, for a perturbation amplitude of $\Psi_{RMP} = 1.1 \times 10^{-5}\,\mathrm{Tm}^2$.

The increase of the particle transport coefficient was also studied with respect to the width of the 3/2 magnetic island, which can be seen in fig. 3.6. Here the particle diffusivity was kept fixed at $0.4\,\mathrm{m}^2\mathrm{s}^{-1}$ and Ψ_{RMP} was varied between $5.4 \times 10^{-6}\,\mathrm{Tm}^2$ and $3.6 \times 10^{-4}\,\mathrm{Tm}^2$. As expected, the effects on the density gradient are stronger for larger islands.

In contrast to the scan over the diffusivity, the three different cases show a similar dependence on the island width for small amplitudes. This can also be seen in fig. 3.7, where the transport coefficient d^+_{rat} divided by w^4 is plotted against the island width. Here the three curves are almost constant for small island widths indicating $d^+_{rat} \propto w^4$. The strongest effects on particle transport in the w^4-regime are observed with the polarization drift model, only considering background transport leads to the smallest effects. The factors relating the configurations A and B to the case configuration C are:

$$d^+_B \approx 1.4 \cdot d^+_C$$
$$d^+_A \approx 2.2 \cdot d^+_C$$

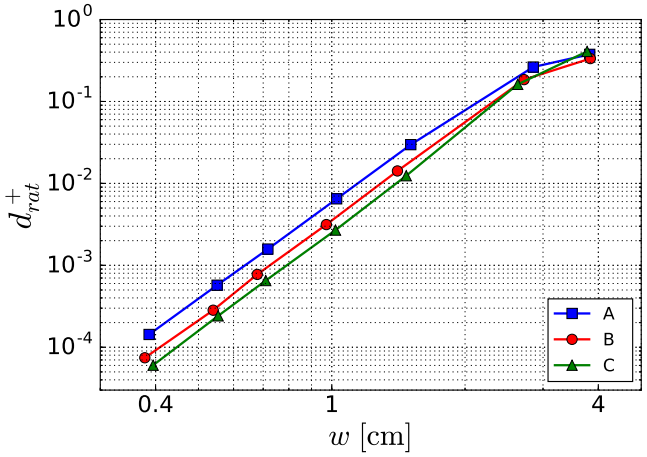

Figure 3.6: The increase of the particle transport coefficient, d^+_{rat}, as a function of the magnetic island width w. The perpendicular particle diffusivity was set to $D_\perp = 0.4\,\mathrm{m^2 s^{-1}}$.

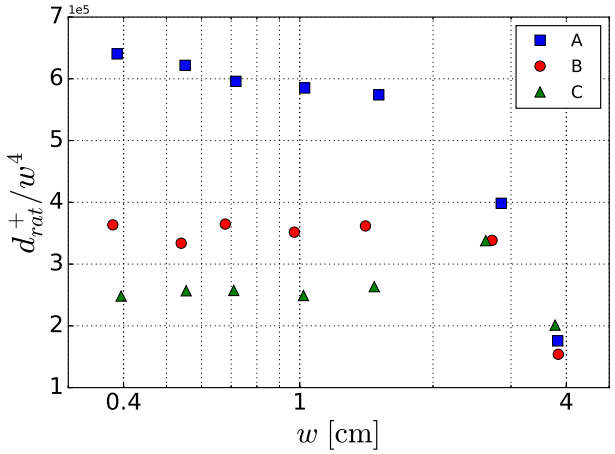

Figure 3.7: The increase of the particle transport coefficient, divided by w^4, as a function of the magnetic island width w. The perpendicular particle diffusivity was set to $D_\perp = 0.4\,\mathrm{m^2 s^{-1}}$.

For larger islands, there is a significant drop in fig. 3.7, corresponding to a kink in fig. 3.6, which shows a change in the w-dependency. This behavior is similar to the temperature flattening by anisotropic heat transport across magnetic islands, where the effective radial heat diffusivity is proportional to w^4 for small islands and proportional to w^2 for large islands [42]. Furthermore, for small island sizes, polarization and diamagnetic effects increase particle transport, but for larger islands they seem to decrease particle transport.

For case C there seems to be an increase of d^+_{rat}/w^4 where the w-dependency changes, which is not the case for A and B. However, when plotting the points with respect to the perturbation amplitude (fig. 3.8 and fig. 3.9), all three configurations show a similar behavior in the transition region at $\Psi_{RMP} = 1.8 \times 10^{-4}\,\mathrm{Tm}^2$, indicating that this behavior is not a consequence of a simulation or calculation error. However, the behavior could be caused by simplifications made for this test case, in particular by neglecting effects caused by temperature changes, which can also affect the density. Therefore, this transition region has to be studied in more depth in the future to come to a consistent conclusion.

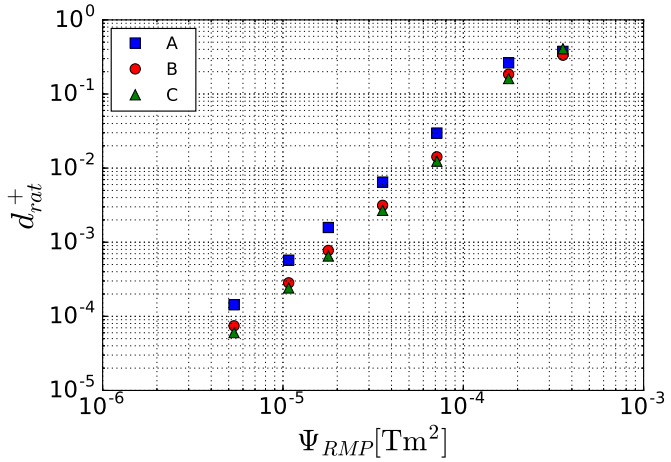

Figure 3.8: The increase of the particle transport coefficient, d^+_{rat}, as a function of the perturbation amplitude Ψ_{RMP}. The perpendicular particle diffusivity was set to $D_\perp = 0.4\,\mathrm{m}^2\mathrm{s}^{-1}$.

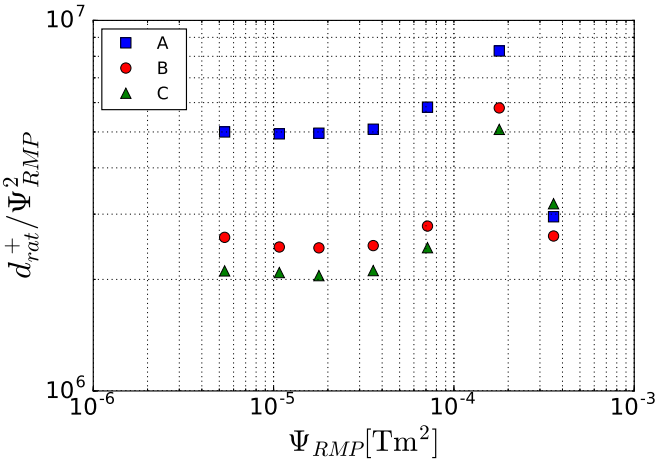

Figure 3.9: The increase of the particle transport coefficient, divided by Ψ_{RMP}^2, as a function of the perturbation amplitude. The perpendicular particle diffusivity was set to $D_\perp = 0.4\,\mathrm{m}^2\mathrm{s}^{-1}$.

Finally, fig. 3.10 and fig. 3.11 show the central density in steady state for the three cases A, B and C. As before, the values are plotted with respect to the axisymmetric simulations, both as a function of the perturbation amplitude (fig. 3.10) and of the particle diffusivity (fig. 3.11). The polarization drift is shown to increase particle loss at the center for all studied cases, consistent with the change in the density gradient (fig. 3.4). Similar to before, these effects grow with higher RMP amplitude and lower particle diffusivity. Furthermore, there seems to be a much stronger dependence on the particle diffusivity than on the perturbation amplitude for the studied cases. The obtained results suggest that polarization drift effects increase the density pump-out in toroidal plasmas accompanying the application of RMP fields, although in the studied test case this pump-out effect is in general much smaller than in experiments (see sec. 1.4.2). This could be a result of the simplifications used for the test case. In our case, only a single RMP mode was used, which resulted in only two islands at the 3/2 and 4/2 rational surfaces. In an experimental setup with finite number of coils, the perturbation would span over a broad spectrum of different mode numbers [29]. Furthermore, the circular plasma shape and comparably large aspect ratio hinders effective mode coupling. Realistic plasma shaping would, together with the RMP spectrum, result in a high number of small islands in the edge region. An increased density gradient, together with a low expected diffusivity in the edge transport barrier region, might lead to a significant overall pump-out effect.

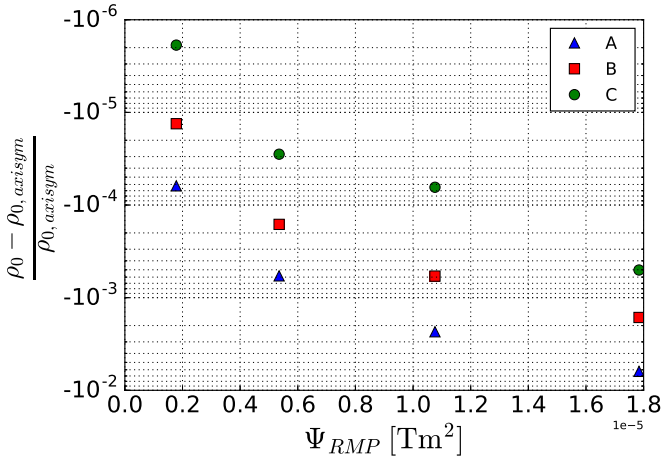

Figure 3.10: Density difference between axisymmetric and non-axisymmetric simulations, normalized to the axisymmetric value, at the magnetic axis ($\Psi_N = 0$) in steady state after RMP application, as a function of the perturbation amplitude. The labels A–C correspond to the definitions used in tab. 3.1.

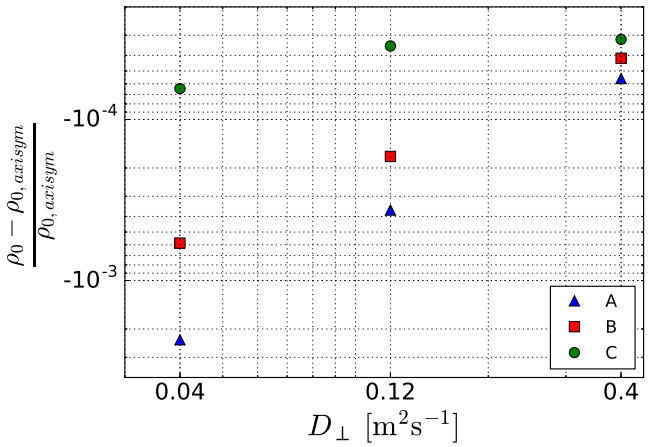

Figure 3.11: Density difference between axisymmetric and non-axisymmetric simulations, normalized to the axisymmetric value, at the magnetic axis ($\Psi_N = 0$) in steady state after RMP application, as a function of the perpendicular particle diffusivity. The labels A–C correspond to the definitions used in tab. 3.1.

Conclusion and Discussion

Understanding non-linear plasma response to externally applied resonant magnetic perturbations is important for extrapolating current experimental results to ITER. Plasma instabilities like edge localized modes limit plasma confinement in tokamak devices and potentially damage plasma facing components. RMPs have been shown to mitigate or fully suppress ELMs and will be the main method for ELM control in ITER. However, the accompanied density pump-out observed in experiments deviates from MHD simulations. In cylindrical geometry, the polarization drift, commonly neglected in simulations, has been shown before to enhance particle transport and induce a density pump-out.

In this thesis, the effects of RMP induced particle transport are extensively studied in toroidal plasmas. For this purpose the non-linear MHD code JOREK was adapted to prepare future comparison with the MHD code TM1.f, which showed the density pump-out in cylindrical geometry and has recently been extended to include toroidal mode coupling. A large number of different simulations was run to cover a wide range of the perturbation amplitude and the particle diffusivity. The extended JOREK model including polarization drift effects was compared to a model only considering diamagnetic effects, and to a model neglecting both.

The polarization drift is shown to have strong effects on the local density gradient at rational surfaces. Although the accompanied density pump-out in the studied test case is small when compared to experiments, the observed effects could lead to larger pump-outs in different conditions, which more closely resemble experimental setups. The obtained results show a strong increase of the pump-out effect at low diffusivities, and in the edge transport barrier in H-mode plasmas the diffusion coefficient is expected to be low. Furthermore, only a single perturbation mode ($m/n = 3/2$) was used for our test case, inducing only a 3/2 and 4/2 magnetic island. In experiments, the finite number of coils leads to a broad spectrum of different RMP perturbations. A realistic plasma shaping would also result in stronger mode coupling, which, together with the broad RMP spectrum, would cause a large number of small islands in the edge region. If the density gradient is significantly increased due to polarization drift effects, the overall pump-out effect could be significant. Thus, the polarization drift might be able to significantly influence the density profile

in realistic cases. Full validation of the model and applications to realistic cases have to be left for the future.

Appendix A

Additional Figures

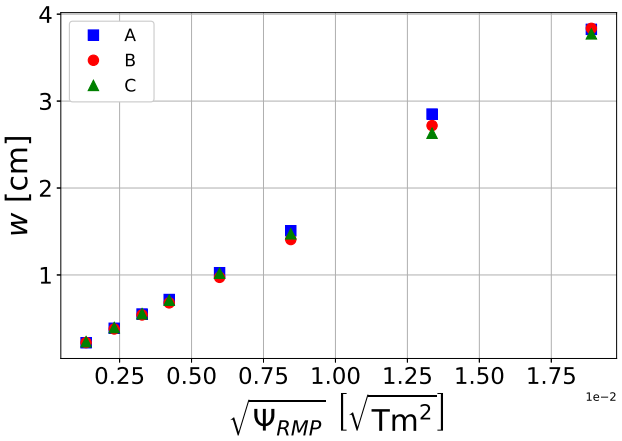

Figure A.1: Plot of the magnetic island width w with respect to the square root of the perturbation flux for all three cases A, B and C (cf. fig. 3.2) and with $D_\perp$ set to $0.4\,\mathrm{m^2 s^{-1}}$.

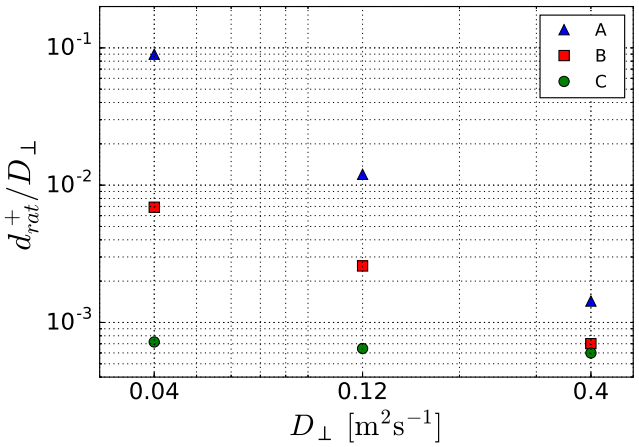

Figure A.2: The relative increase of the transport coefficient, $d^{+}_{rat}/D_{\perp}$, corresponding to the change in the normalized density gradient, $1 - \left(\frac{\partial \rho}{\partial \Psi_N}\right) / \left(\frac{\partial \rho_{axisym}}{\partial \Psi_N}\right)$, plotted against the perpendicular particle diffusivity. (cf. fig. 3.5)

Bibliography

[1] M. Kaufmann. *Plasmaphysik und Fusionsforschung*. 2. Auflage. Springer-Verlag GmbH, 2013. ISBN: 3-658-03238-8.

[2] U. Stroth. *Plasmaphysik: Phänomene, Grundlagen und Anwendungen*. 2. Auflage. Springer-Verlag GmbH. ISBN: 3-662-55236-0.

[3] F. Cap. *Lehrbuch der Plasmaphysik und Magnetohydrodynamik*. Springer-Verlag GmbH, 1994. ISBN: 3-7091-6622-2. DOI: 10.1007/978-3-7091-6622-2.

[4] K. H. Spatschek. *Theoretische Plasmaphysik*. B. G. Teubner Stuttgart, 1990. ISBN: 3-519-03041-1.

[5] ASDEX Team. »The H-Mode of ASDEX«. In: 29 (July 2018).

[6] G. T. A. Huijsmans et al. »Modelling of edge localised modes and edge localised mode control«. In: *Physics of Plasmas* 22.2 (2015), p. 021805. DOI: 10.1063/1.4905231.

[7] A. Loarte et al. In: *Proc. 23rd Int. Conf. on Fusion Energy* (2010).

[8] P. T. Lang et al. »High density H-mode operation by pellet injection and ELM mitigation with the new active in-vessel saddle coils in ASDEX Upgrade«. In: *Proc. 38th EPS Conf. on Plasma Physics* (2011).

[9] S H Kim et al. »Comparing magnetic triggering of ELMs in TCV and ASDEX Upgrade«. In: *Plasma Physics and Controlled Fusion* 51.5 (2009), p. 055021. URL: http://stacks.iop.org/0741-3335/51/i=5/a=055021.

[10] H. R. Strauss et al. »ELM simulations with M3D«. In: *APS Meeting Abstracts*. Oct. 2006, BP1.021.

[11] H. R. Strauss et al. »Studies of ELMs and RMPs with M3D«. In: *APS Meeting Abstracts*. Nov. 2007, GP8.098.

[12] B D Dudson et al. »Simulation of edge localized modes using BOUT++«. In: *Plasma Physics and Controlled Fusion* 53.5 (2011), p. 054005. URL: http://stacks.iop.org/0741-3335/53/i=5/a=054005.

[13] A Y Pankin et al. »Modelling of ELM dynamics for DIII-D and ITER«. In: *Plasma Physics and Controlled Fusion* 49.7 (2007), S63. URL: http://stacks.iop.org/0741-3335/49/i=7/a=S04.

[14] F. Orain. »Pump-out study in JOREK«. In: (2014).

[15] F.J. Artola et al. »Non-linear magnetohydrodynamic simulations of edge localised mode triggering via vertical position oscillations in ITER«. In: *Nuclear Fusion* 58.9 (2018), p. 096018. URL: http://stacks.iop.org/0029-5515/58/i=9/a=096018.

[16] Hoelzl M. et al. »Insights into type-I edge localized modes and edge localized mode control from JOREK non-linear magneto-hydrodynamic simulations«. In: *Contributions to Plasma Physics* 0.0 (). DOI: 10.1002/ctpp.201700142.

[17] François Orain et al. »Non-linear MHD modeling of edge localized mode cycles and mitigation by resonant magnetic perturbations«. In: *Plasma Physics and Controlled Fusion* 57.1 (2015), p. 014020. URL: http://stacks.iop.org/0741-3335/57/i=1/a=014020.

[18] D. Meshcheriakov et al. »Tearing mode seeding by externally provided resonant magnetic perturbations«. In: *Proc. 44th EPS Conf. on Plasma Physics* (2017).

[19] D. Meshcheriakov et al. »Tearing mode seeding by external magnetic perturbations«. In: *Proc. 45th EPS Conf. on Plasma Physics* (2018).

[20] Yueqiang Liu et al. »ELM control with RMP: plasma response models and the role of edge peeling response«. In: *Plasma Physics and Controlled Fusion* 58.11 (2016), p. 114005. URL: http://stacks.iop.org/0741-3335/58/i=11/a=114005.

[21] T.C. Hender et al. »Effect of resonant magnetic perturbations on COMPASS-C tokamak discharges«. In: *Nuclear Fusion* 32.12 (1992), p. 2091. URL: http://stacks.iop.org/0029-5515/32/i=12/a=I02.

[22] M. Becoulet et al. »Screening of resonant magnetic perturbations by flows in tokamaks«. In: *Nuclear Fusion* 52.5 (2012), p. 054003. URL: http://stacks.iop.org/0029-5515/52/i=5/a=054003.

[23] T.E. Evans et al. »RMP ELM suppression in DIII-D plasmas with ITER similar shapes and collisionalities«. In: *Nuclear Fusion* 48.2 (2008), p. 024002. URL: http://stacks.iop.org/0029-5515/48/i=2/a=024002.

[24] W. Suttrop et al. »Full suppression of Edge Localised Modes with non-axisymmetric magnetic perturbations at low plasma edge collisionality in ASDEX Upgrade«. In: *Proc. 44th EPS Conf. on Plasma Physics* (2017). URL: http://ocs.ciemat.es/EPS2017PAP/pdf/P5.127.pdf.

[25] M. Valovič et al. »Pellet refuelling of particle loss due to ELM mitigation with RMPs in the ASDEX Upgrade tokamak at low collisionality«. In: *Nuclear Fusion* 56.6 (2016), p. 066009. URL: http://stacks.iop.org/0029-5515/56/i=6/a=066009.

[26] E. Nardon et al. »ELM Control by Resonant Magnetic Perturbations on JET and MAST«. In: *Proc. HTPD High Temperature Plasma Diagnostics* (2008).

[27] A. Kirk et al. »Understanding edge-localized mode mitigation by resonant magnetic perturbations on MAST«. In: *Nuclear Fusion* 53.4 (2013), p. 043007. URL: http://stacks.iop.org/0029-5515/53/i=4/a=043007.

[28] Y Liang et al. »Active control of type-I edge localized modes on JET«. In: *Plasma Physics and Controlled Fusion* 49.12B (2007), B581. URL: http://stacks.iop.org/0741-3335/49/i=12B/a=S54.

[29] F. Orain et al. »Non-linear modeling of the plasma response to RMPs in ASDEX Upgrade«. In: *Nuclear Fusion* 57.2 (2017), p. 022013. URL: http://stacks.iop.org/0029-5515/57/i=2/a=022013.

[30] E. Nardon et al. »Quasi-linear MHD modelling of H-mode plasma response to resonant magnetic perturbations«. In: *Nuclear Fusion* 50.3 (2010), p. 034002. URL: http://stacks.iop.org/0029-5515/50/i=3/a=034002.

[31] A. Kirk et al. »Resonant magnetic perturbation experiments on MAST using external and internal coils for ELM control«. In: *Nuclear Fusion* 50.3 (2010), p. 034008. URL: http://stacks.iop.org/0029-5515/50/i=3/a=034008.

[32] A Kirk et al. »Magnetic perturbation experiments on MAST L- and H-mode plasmas using internal coils«. In: *Plasma Physics and Controlled Fusion* 53.6 (2011), p. 065011. URL: http://stacks.iop.org/0741-3335/53/i=6/a=065011.

[33] M. Z. Tokar et al. »Particle transfer in edge transport barrier with stochastic magnetic field«. In: *Physics of Plasmas* 15.7 (2008), p. 072515. DOI: 10.1063/1.2959122.

[34] Q. Yu and S. Günter. »Plasma response to externally applied resonant magnetic perturbations«. In: *Nuclear Fusion* 51.7 (2011), p. 073030. URL: http://stacks.iop.org/0029-5515/51/i=7/a=073030.

[35] F.L. Waelbroeck et al. »Role of singular layers in the plasma response to resonant magnetic perturbations«. In: *Nuclear Fusion* 52.7 (2012), p. 074004. URL: http://stacks.iop.org/0029-5515/52/i=7/a=074004.

[36] F. Orain. *private communication*. 2018.

[37] F. Orain et al. »Non-linear magnetohydrodynamic modeling of plasma response to resonant magnetic perturbations«. In: *Physics of Plasmas* 20.10 (2013), p. 102510. DOI: 10.1063/1.4824820.

[38] Q. Yu, S. Günter and K. Lackner. »Suppressing magnetic island growth by resonant magnetic perturbation«. In: *Nuclear Fusion* 58.5 (2018), p. 054003. URL: http://stacks.iop.org/0029-5515/58/i=5/a=054003.

[39] Q. Yu, S. Günter and K. Lackner. »Numerical modelling of sawtooth crash using two-fluid equations«. In: *Nuclear Fusion* 55.11 (2015), p. 113008. URL: http://stacks.iop.org/0029-5515/55/i=11/a=113008.

[40] Q. Yu et al. »Seed island formation by forced magnetic reconnection«. In: *Nuclear Fusion* 52.6 (2012), p. 063020. URL: http://stacks.iop.org/0029-5515/52/i=6/a=063020.

[41] Q. Yu and S. Günter. »Locking of neoclassical tearing modes by error fields and its stabilization by RF current«. In: *Nuclear Fusion* 48.6 (2008), p. 065004. URL: http://stacks.iop.org/0029-5515/48/i=6/a=065004.

[42] Matthias Hölzl. »Diffusive Heat Transport across Magnetic Islands and Stochastic Layers in Tokamaks«. Dissertation. München: Technische Universität München, 2010.

Acknowledgments

I would like to thank everyone who supported me during the course of this bachelor thesis, especially:

Sibylle Günter for giving me the opportunity to work on this bachelor thesis at IPP Garching and taking the time to discuss my work. Matthias Hölzl for guiding me through this thesis, helping with major and minor problems and always finding time in his tight schedule. Qingquan Yu for providing the input parameters for our test case, taking the time for discussions and giving many helpful tips. François Orain for providing the JOREK model used for my thesis and finding the time to discuss my results. The JOREK team at IPP, especially Dmytro Meshcheriakov for reading through my work and discussing the theoretical background, and Fabian Wieschollek for helping me get started with JOREK and answering any technical questions.